AGU PUBLICATIONS

JGR

Journal of Geophysical Research: Solid Earth

RESEARCH ARTICLE
10.1002/2017JB014855

Key Points:
- Volcano dimensions as indicators of the plumbing system
- Volcano topography modeled as a pile of lavas emitted from a single vent
- Estimations of depth and size of magma chamber from inversion of lava dimensions and volcano topography

Supporting Information:
- Supporting Information S1

Correspondence to:
A. Castruccio,
acastruc@ing.uchile.cl

Citation:
Castruccio, A., Diez, M., & Gho, R. (2017). The influence of plumbing system structure on volcano dimensions and topography. *Journal of Geophysical Research: Solid Earth*, *122*, 8839–8859. https://doi.org/10.1002/2017JB014855

Received 11 AUG 2017
Accepted 11 OCT 2017
Accepted article online 14 OCT 2017
Published online 3 NOV 2017

The Influence of Plumbing System Structure on Volcano Dimensions and Topography

Angelo Castruccio[1,2], Mikel Diez[3], and Rayen Gho[1,2]

[1]Departamento de Geología, Universidad de Chile, Santiago, Chile, [2]Centro de Excelencia en Geotermia de los Andes, Santiago, Chile, [3]School of Earth Sciences, University of Bristol, Bristol, UK

Abstract Volcano morphology has been traditionally studied from a descriptive point of view, but in this work we took a different more quantitative perspective. Here we used volcano dimensions such as height and basal radius, together with the topographic profile as indicators of key plumbing system properties. We started by coupling models for the ascent of magma and extrusion of lava flows with those for volcano edifice construction. We modeled volcanic edifices as a pile of lavas that are emitted from a single vent and reduce in volume with time. We then selected a number of arc-volcano examples to test our physical relationships and estimate parameters, which were compared with independent methods. Our results indicate that large volcanoes (>2,000 m height and base radius >10 km) usually are basaltic systems with overpressured sources located at more than 15 km depth. On the other hand, smaller volcanoes (<2,000 m height and basal radius <10 km) are associated with more evolved systems where the chambers feeding eruptions are located at shallower levels in the crust (<10 km). We find that surface observations on height and basal radius of a volcano and its lavas can give estimates of fundamental properties of the plumbing system, specifically the depth and size of the magma chamber feeding eruptions, as the structure of the magmatic system determines the morphology of the volcanic edifice.

1. Introduction

One of the fundamental properties of a volcanic edifice is its morphology (Davidson & De Silva, 2000), but surprisingly, little work has been done to explain the main plumbing system properties controlling it and most of the work on volcano morphology has been focused on morphometric analyses (e.g., Grosse et al., 2014; Karatson et al., 2010; Wood, 1978) with few hints on the key control parameters. Primary volcano morphology is the sum of the erupted products from a vent. The magma extrusion rate and erupted volume during a volcanic eruption depends on factors such as depth and size of the magma chamber, the viscosity, density, and volatile content of the magma and the conduit dimensions and pressure gradient (e.g., Slezin, 2003; Wadge, 1981; Woods, 1995). Thus, volcano morphology should reflect the evolution of these internal properties of the magma system feeding a volcano.

The study of such magmatic system properties of a volcano is fundamental to understand the processes controlling its eruptive activity. These properties are commonly constrained employing methods such as geothermobarometry (e.g., Putirka, 2008) and seismic tomography (e.g., Lees, 2007). In contrast, comparatively fewer works have tried to study the mechanisms and magma system conditions that influence the growth and dimensions of a volcano (e.g., Ben-Avraham & Nur, 1980; Borgia & Linneman, 1992; Lacey et al., 1981; Stasiuk & Jaupart, 1997; Wilson et al., 1992). Here we take this line of inquiry.

Current advances in studies on volcanic processes have made it possible to infer extrusion rates of individual eruptions from field data of fall deposits (e.g., Alfano et al., 2011; Bonadonna et al., 2015; Carey & Sparks, 1986) or lava flows (e.g., Castruccio & Contreras, 2016; Deardoff & Cashman, 2012), but much less work has been carried out to infer plumbing system properties from these data or to analyze extrusion rate trends in the evolution of a volcano.

During many effusive eruptions, the effusion rate typically decays quickly after reaching its peak, a phenomenon attributed to the release of the overpressure in the magma chamber due to the evacuation of magma (Blake, 1981; Wadge, 1981; Woods & Huppert, 2003). Thus, data on erupted volume versus time during an eruption can give some hints of the magma system properties. However, this information is, in general, insufficient to reasonably constrain all key parameters, since further properties such as magma

chamber depth and size and conduit dimensions are not known and additional relationships between them are necessary.

A common occurrence in many composite volcanoes in subduction zones is the reduction through time of the maximum length and volume of the emitted lava flows (e.g., Borgia & Linneman, 1992; Carrasco-Nuñez, 1997; Clavero et al., 2004; Sparks et al., 2008). This pattern could indicate that the growth of the volcano is reducing the pressure gradient driving the magma to ascend out of the magma chamber, decreasing the magnitude and intensity of the eruptions. Pinel and Jaupart (2000, 2004) and Pinel, Jaupart, and Albino (2010) have shown the importance that the load exerted by the volcanic edifice could have on the magmatic system, arguing that it could control the periodicity, extruded volume, and composition of the eruptions. A control of vent elevation on erupted volume is also suggested by data from historical eruptions at some volcanoes. For example, Epp et al. (1983) noted an inverse correlation between vent elevation and erupted volume at Kilauea volcano for eruptions between 1955 and 1979. At Klyuchevskoy volcano, Russia, the largest lava flow of the twentieth century was emitted from a vent located more than 3,000 m below the summit vent (Fedotov & Zharinov, 2007). At Etna volcano, the largest historical lava flow was emitted in 1669 from a flank vent located ~2,400 m below the summit of the volcano (Branca et al., 2013). Consequently, the interplay of volcano height with erupted volumes and extrusion rates could give us the additional information needed to infer the most important magmatic system properties driving eruptions.

In this work we investigate the influence of the plumbing system properties on the morphology and dimensions that a volcano can attain. We first develop a model for the extrusion of lava flows from a single magma chamber. The volume of a lava flow depends on size and location of magma chamber, magma density and viscosity, magma overpressure, and crustal density profile. We then analyze the influence of these factors on volcano morphology. Here we are considering a volcano as a simple cone, composed by a pile of lava flows and not affected by volcanic avalanches, caldera collapses, vent migration, or climate conditions. We tested some of our hypotheses with data from some arc volcanoes, where we used data from eruptions, emitted volumes of lavas, and volcano topographic profiles to estimate plumbing system parameters. Our results reveal that these parameters are a first-order control on volcano morphology, and consequently, surface observations of volcanic products and edifice dimensions can give insights and constrains into the plumbing system of a volcano.

2. Physical Modeling of Ascent of Magma, Lava Volumes, and Volcano Dimensions

In this section we develop a series of physical relationships between plumbing system properties and lava extrusion and the construction and dimensions of a volcano. Any such model should start with the adequate simplifications in order to get the insights we want to explore which would be impossible with a too complex model. The following equations should be seen as a starting point to understand magmatic systems—volcano edifice interactions and further complexities should be incorporated in future works. In the same line, our results and examples shown in the next sections should be seen as semiquantitative and for comparison purposes, as some parameters such as critical overpressure, magma chamber geometry or magma, and host rock bulk modulus are poorly constrained for volcanic systems, and we used fixed values for them.

We first analyze the internal factors controlling the extrusion and volume of individual lava flows. Then we investigate the construction and morphology of a volcano edifice resulting from a pile of lavas emitted from a single source. Finally, we studied the additional influence of a deep reservoir on the maximum dimensions that a volcano can attain.

2.1. Extrusion and Dimensions of Lava Flows

We start considering the ascent of magma from a magma chamber of volume V_c, with its top located at a depth H below the surface (Figure 1). We assume laminar flow conditions and no fragmentation of magma. According to Stasiuk and Jaupart (1997), these assumptions are valid for lava eruptions with small quantities of volatiles. In the next sections we discuss the implications and validity of our simplifications. Under these conditions, the volumetric flow rate Q of the ascending magma in a dike is given by (Munson et al., 1990)

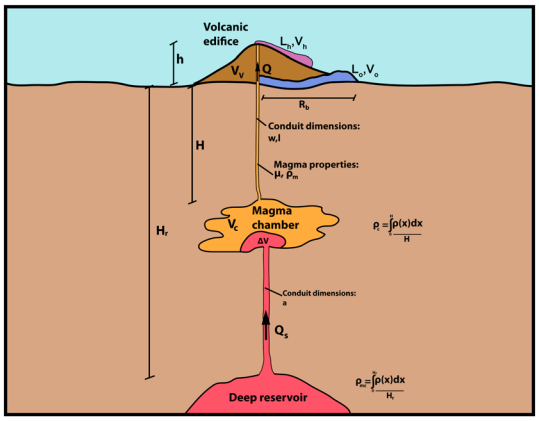

Figure 1. Cartoon (not to scale) showing the extrusion of a lava flow from a magma chamber located at a depth *H* and with parameters used in this work.

$$Q = \frac{w^3 l}{12\mu}\left(\Delta\rho g + \frac{\Delta P}{H}\right), \quad (1)$$

where w and l are the dike width and length, respectively, and μ is the magma viscosity. We also assume $w \ll l$. The first term in parentheses is associated with magma buoyancy, where $\Delta\rho$ is the difference between the mean density of the crust, ρ_c $(= \frac{1}{H}\int_0^H \rho(x)dx$, where x is the vertical coordinate and 0 is the surface level), above the magma chamber and magma density, ρ_m. The g is the gravitational acceleration. The second term is the pressure gradient generated by the overpressure of the magma chamber, ΔP, over lithostatic pressure (a list of symbols is found in Table 1). For a cylindrical conduit, $w^3 l/12\ \mu$ is replaced by $\pi r^4/8\ \mu$ where r is the radius of the conduit. Wadge (1981) derived a similar equation, but without considering magma buoyancy. Stasiuk and Jaupart (1997) used the same expression, but only with a cylindrical geometry and with an additional term between parentheses due to the load of the erupted lava at the surface.

Table 1
List of Parameters Used in the Equations of the Main Text

Symbol	Parameter	Units
μ	magma viscosity	Pa s
a	radius of conduit connecting deep reservoir and magma chamber	m
F_{ms}	fraction of initial flow rate Q_s	
g	gravity acceleration	m/s^2
H	depth of top of magma chamber	m
h	height of volcano edifice	m
h_{max}	maximum height of volcano edifice	m
H_r	depth of top of deep reservoir	m
κ'	effective bulk modulus (combined bulk modulus of magma and host rock)	Pa
l	length of a dike	m
L	length of a lava flow	m
L_{max}	maximum length of an individual lava flow	m
n	number of lavas building a volcano	
Q	effusion rate of an eruption	m^3/s
Q_0	effusion rate of an eruption with no edifice	m^3/s
Q_h	effusion rate of an eruption from an edifice of height h	m^3/s
Q_s	flow rate from a deep reservoir to a magma chamber	m^3/s
r	radius of a cylindrical conduit connecting magma chamber and surface	m
R_{bas}	basal radius of a volcano	m
T	thickness of a lava flow	m
V_0	volume of a lava emitted from a vent without edifice	m^3
V_c	volume of magma chamber	m^3
V_e	erupted volume of a single eruption	m^3
V_h	volume of a lava emitted from a vent located at height h above basal level	m^3
w	width of a dike	m
W	width of a lava flow	m
α	shape factor of topographic profile	m^2
ΔP	overpressure inside a magma chamber	Pa
ΔP_i	critical overpressure to trigger an eruption	Pa
ΔV	additional volume of magma inside a magma chamber	m^3
ΔV_i	additional volume of magma inside a magma chamber needed to trigger an eruption	m^3
$\Delta\rho$	density difference between magma and crust	kg/m^3
ρ_c	mean density of crust	kg/m^3
ρ_m	mean density of magma	kg/m^3
Φcrit	critical slope of a volcano	degrees

We assume that the overpressure inside the magma chamber is built up by the injection of new magma into it (Blake, 1981), such that

$$\Delta \mathrm{P} = \frac{\Delta \mathrm{V}}{V_c}\kappa', \tag{2}$$

where ΔV is the additional volume of magma injected into the reservoir and κ' is the effective bulk modulus, a term that incorporates the effects of the bulk modulus of magma and the surrounding wall rock (Huppert & Woods, 2002). A typical value for κ' for low crystal and volatile content is 5×10^9 Pa (Huppert & Woods, 2002), which we used for all further calculations, unless stated otherwise. Here we are not considering the overpressure generated by the buoyancy of the magma inside the chamber or the volumetric expansion due to volatile exsolution, as these effects would be important for large, shallow reservoirs (e.g., Blake, 1984; Jellinek, 2014) associated to large, caldera-forming eruptions. In our analysis we are assuming that a fracture is propagated to the surface and an eruption occurs once a critical overpressure ΔP_i is reached. The complex problem of dike propagation in a volcanic system has been studied by many authors (e.g., Gudmundsson, 2006; Kavanagh & Sparks, 2011; Lister & Kerr, 1991; Rubin, 1993), but there are some unsolved problems that complicate this issue. Commonly, an elastic medium is assumed, but the ascent zone in a mature volcanic system is probably heated up and previously fractured. Additionally, some studies have shown the difficulty of matching field observations with simple elastic theory (e.g., Daniels et al., 2012). For these reasons we restrict ourselves to assuming that an eruption will occur for a fixed ΔP_i.

After the onset of an eruption, due to the evacuation of magma from the chamber, ΔV varies as

$$\Delta \mathrm{V}(t) = \Delta V_i - V_e(t), \tag{3}$$

where ΔV_i is the initial additional injected volume of magma inside the chamber that generated the overpressure ΔP_i and $V_e(t)$ is the erupted volume at time t. Replacing equation (3) into (2) and then equation (2) into (1) we obtain

$$\frac{dV_e(t)}{dt} = A - BV_e(t), \tag{4}$$

where

$$\frac{dV_e(t)}{dt} = Q(t), A = \frac{w^3 I}{12\mu}\left(\Delta \rho g + \frac{\kappa' \Delta V_i}{V_c H}\right) \text{and } B = \frac{w^3 I}{12\mu}\frac{\kappa'}{V_c H}.$$

Equation (4) can be solved analytically, and $Q(t)$ becomes an exponential function (Wadge, 1981):

$$\frac{dV_e(t)}{dt} = A\exp(-Bt), \tag{5}$$

and the total erupted volume is A/B:

$$\frac{A}{B} = V_e(t \to \infty) = \frac{V_c}{\kappa'}(\Delta P_i + \Delta \rho g \mathrm{H}). \tag{6}$$

In the case that the conduit dimensions or the viscosity are dependent on time or space during an eruption, then equation (4) would be more complex and may not be solved analytically but only numerically.

If we know the variation of the effusion rate with time during an eruption or equivalently the accumulated volume versus time, we can fit the data of the eruption with equations (5) or (6) by adjusting parameters A and B.

Additional information on the plumbing system can be obtained by analyzing the effects of a volcanic edifice of height h (Figure 1) on the ascent of magma and eruption. In this case, the conduit length will be $H + h$, and the hydrostatic pressure that the magma inside the conduit is exerting at the base of it will be $\rho_m g(H + h)$. If the magma chamber is deep enough, the lithostatic pressure at the chamber level will not be affected by the volcanic edifice (Pinel & Jaupart, 2000). According to these authors, the effects of the edifice will be felt down to a depth of 3 R_b, where R_b is the radius of the edifice. However, the same results of these authors indicate that for a depth of just R_b the additional normal stress caused by the edifice is only ~0.25% (~9.5% for 0.5 R_b)

of the stress caused by the total weight of the edifice at the base. Considering the volcano edifice, equation (1) is rewritten as

$$Q = \frac{w^3 l}{12\mu}\left(\frac{\Delta\ \rho g H + \Delta P - \rho_m g h}{H + h}\right). \tag{7}$$

The erupted volume in this case would be

$$V_e(t\to\infty) = \frac{V_c}{\kappa'}(\Delta P_i + \ \Delta\ \rho g H - \rho_m g h). \tag{8}$$

Now let us consider two lava flows emitted at different stages during the construction of a volcano cone (Figure 1). L_0 was emitted at the beginning of the buildup of the volcano, when there was no edifice and L_h was emitted through the summit when the volcano had a height h. If Q_0 is the initial effusion rate of L_0 and Q_h is the initial effusion rate of L_h, then the ratio Q_h/Q_0 is (assuming the same magma viscosity and conduit dimensions, and noting that the ratio is the same if we consider mean effusion rate instead of initial effusion rate)

$$\frac{Q_h}{Q_0} = \frac{H}{H + h}\left(1 - \frac{\rho_m g h}{\Delta\rho g H + \Delta P_i}\right). \tag{9}$$

Additionally, the ratio between the volume of lava L_h, V_h, and the volume of lava L_0, $V_{0,}$ has the form

$$\frac{V_h}{V_0} = 1 - \left(\frac{\rho_m g h}{\Delta\rho g H + \Delta P_i}\right). \tag{10}$$

We can solve for the parameters H, V_c, and conduit dimensions as follows, using the values of κ' and μ, plus measurements of h and ρ_m and using the erupted volume versus time data during the evolution of a single eruption of a volcano (to obtain parameters A and B), with the additional information of erupted volumes and effusion rates of lavas at different stages of the volcano construction (equations (9) and (10)):

First, we replace (6) in (10):

$$\frac{V_h}{V_0} = 1 - \left(\frac{B V_c \rho_m g h}{A\kappa'}\right) \tag{11}$$

and rearranging for V_c, we obtain

$$V_c = \frac{A\kappa'}{B\rho_m g h}\left(1 - \frac{V_h}{V_0}\right). \tag{12}$$

Next, notice that from (9) and (10) results

$$\frac{Q_h}{Q_0} = \frac{H}{H + h}\frac{V_h}{V_0} \tag{13}$$

and solving for H gives

$$H = h\left(\frac{V_0 Q_h}{Q_0 V_h - V_0 Q_h}\right). \tag{14}$$

From B in (4) we can write

$$w^3 l = \frac{12\mu B V_c H}{\kappa'}. \tag{15}$$

Thus, if we know μ, we can obtain the product $w^3 l$ for a dike or r for a cylindrical conduit.

Although the cases of Kilauea, Etna, and Klyushevskoy volcanoes mentioned in the introduction suggest a strong control of vent height on erupted volume, equation (8) shows that variations of erupted volumes of lavas also depend on volume changes of the magma chamber, shifts of magma chamber position, or changes of ΔP_i or κ'. It is out of the scope of this work to analyze all these factors, although they should be considered in future works.

In principle, equations (12), (14), and (15) allow us to solve for V_c, H, and conduit dimensions measuring the ratios Q_h/Q_0 and V_h/V_0 plus the erupted volume versus time during a single eruption and using estimations of μ, ρ_c, and κ and measurements of h and ρ_m. Figure S1 in the supporting information shows the sensitivity of V_c, H, and w for some of these parameters. This figure shows, however, that the ratio Q_h/Q_0 is of little practical use. First, we are assuming that conduit dimensions and viscosities are constant through different eruptions. Although we can estimate variations of viscosities (using chemical compositions and crystal contents) the estimations of possible variations of conduit dimensions in time and space are impossible to constrain by any method at present. Second, although it is possible to make good estimations of the effusion rate of past eruptions using lava morphologies (e.g., Castruccio et al., 2014; Deardoff & Cashman, 2012; Pinkerton & Wilson, 1994), we need high precision estimations, as H is very sensitive to this ratio (Figure S1 in the supporting information). We still can use equations (12) and (15) to get V_c and conduit dimensions if we use H as an input parameter that could be estimated independently by other methods. In the next section we link plumbing system properties with volcano edifice shape and dimensions, where we use volcano height as an indicator of parameter H.

2.2. Volcano Building and Morphometry

Here we develop a relationship between the plumbing system parameters analyzed in the previous section and volcano dimensions and morphology. We relate the maximum height a volcano can attain and its basal radius to these parameters and then we propose a set of equations that links volcano topographic profile with these dimensions. We assume that a volcano is a pile of lavas emitted from a single vent.

A volcano will grow taller until the system is unable to generate a pressure gradient that allows the magma to ascend from the magma chamber to the surface. From equation (7) an eruption will occur only if

$$\Delta \mathrm{P} + \Delta\, \rho \mathrm{gH} - \rho_m g h > 0. \tag{16}$$

This implies that the maximum height, h_{max}, a volcano can attain is

$$h_{\mathrm{max}} = \frac{\Delta \rho}{\rho_m} H + \frac{\Delta P_i}{\rho_m g}. \tag{17}$$

Similar relationships, but written in different form, were mentioned by Davidson and De Silva (2000) and Pinel et al. (2010). Ben-Avraham and Nur (1980) used a slightly different relationship (without overpressure and taking into account ocean depth) to estimate the depth of the magma source. Sparks (1993) used the same expression (without considering overpressure) to estimate the depth of the magmatic source of Hawaiian volcanoes. Wilson et al. (1992) criticized the estimation of source depths through this equation, arguing that volcano height also depends on erupted volumes, eruption frequency, etc. We agree with Wilson et al. (1992) regarding the misuse of the equation to estimate source depths, as magma does not ascend continuously from mantle source to surface. We interpret depths deduced from equation (17) as depths of the magma chamber that triggers the eruption. In subsequent sections our work gives some hints into the role that some of the additional parameters mentioned by Wilson et al. (1992) can have on maximum height. According to equation (17), volcano height depends on magma buoyancy, magma density, magma chamber depth, and the critical overpressure needed to start an eruption. Now let us consider a basaltic magma with a density profile with depth depicted in Figure 2a (with the corresponding exsolution of 2% of H_2O), a critical overpressure of 25 MPa, and a crustal density profile with depth as follows: 0–6 km: 2,600 kg/m^3; 6–20 km: 2,800 kg/m^3; 20–30 km: 2,900 kg/m^3; and 30–40 km: 3,100 kg/m^3 (Figure 2a, profile of the Kamchatka peninsula crust taken from Fedotov, Zharinov, & Gontovaya, 2010). With a magma chamber located at 6 km depth, there is little buoyancy and the volcano height is mainly due to overpressure. In this case the maximum volcano height would be ~1,300 m. If the chamber is located at 20 km, buoyancy effects become noticeable and the maximum height of the volcano would be 2,050 m. At 35 km it would be ~3,450 m (Figure 2b). Notice that subduction stratocones rarely exceed 3 km above their base (Davidson & De Silva, 2000) and we will discuss this issue later.

The basal radius of a volcanic edifice, R_{bas}, will be controlled initially by the length of the first lavas erupted, as these will be the most voluminous ones. The final length of a lava flow is controlled mainly by the effusion

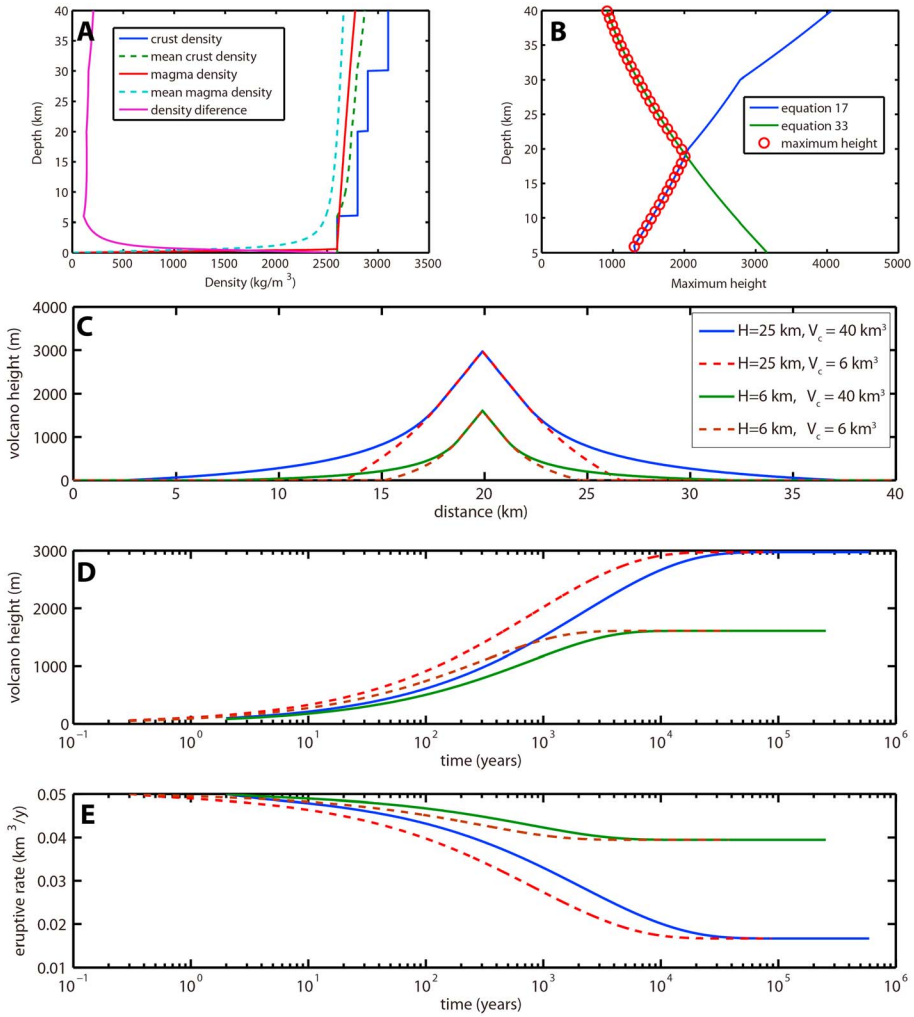

Figure 2. (a) Example of crustal and magma density profiles (and their mean values) with depth. Also shown is the difference between the mean values of magma and crust density. (b) Maximum height that a volcano can attain according to equations (17) and (33) and using the parameters of Figure 2a. (c) Volcano profiles for different conditions of H and V_c. (d) Volcano height evolution through time for the four cases depicted in Figure 2c. (e) Eruptive rate evolution through time for the four cases depicted in Figure 2c (notice that in these cases, the volcano reached its maximum height due to restriction of equation (17) and not equation (33)).

rate and volume (e.g., Harris & Rowland, 2009; Pinkerton & Wilson, 1994; Walker, 1973). As a first-order approximation, the maximum length, L_{max}, of a single lava flow can be written as (Kilburn & Lopes, 1991):

$$L_{max} = CV_e^{0.5}, \tag{18}$$

where C is a coefficient (with dimensions $m^{-1/2}$) that depends mainly on effusion rate, cross sectional area, viscosity, and topography. Notice that we are not dealing with differences between cooling- and volume-limited flows (Harris & Rowland, 2009). For basaltic flows C is on the order of 1 to 2, while for more evolved compositions C is smaller (~0.5; Kilburn & Lopes, 1991). From equations (6) and (18), the basal radius of a volcano can be rewritten as

$$R_{bas} = C\left(\frac{V_c}{\kappa'}(\Delta P_i + \Delta\ \rho g H)\right)^{0.5}. \tag{19}$$

Thus, the maximum height and basal radius of a volcano edifice can be used to estimate H and V_c if we know the values of κ', ΔP_i, ρ_m, and ρ_c.

Now we develop a topographic profile model for a volcanic edifice of height h_{max} and basal radius R_{bas}. First, we consider a volcano as a pile of lavas distributed radially from a central vent. We do not consider the effects of dike intrusions analyzed by Annen et al. (2001). We assume that all lavas have the same dimensions (later we analyze the case with lavas of reduced length with time): L (length), W (width), and T (thickness). Using geometrical considerations, for a sufficiently large number of lava units, the height of a volcano will decrease with distance from the vent as the planimetric area to cover with lavas at a certain distance, r, is proportional to the perimeter of a circle of radius r. This means that at a certain distance r, the ratio between the sum of the widths of all the lavas, nW (with n the number of lavas) and the perimeter, $2\pi r$, is $nW/2\pi r$ and the mean height of the volcano edifice at r will be this ratio multiplied by the thickness of lavas, T:

$$h(r) = \frac{nTW}{2\pi r} \qquad (\text{Valid for } R_{bas} > r > W/2\pi). \tag{20}$$

The relationship should be valid for $r > W/2\pi$ as for a smaller r, the perimeter of the edifice will be less than the width of an individual lava. Notice that the volume of the volcano, V_v, is equal to nLTW and equation (20) can be written as

$$h(r) = \frac{V_v}{2\pi L r} = \frac{D}{r} \quad \text{with} \quad D = \frac{V_v}{2\pi L}. \tag{21}$$

In the scenario where lavas reduce their volume due to the height of the volcano, the topographic profile is (using the same geometrical reasoning)

$$h(r) = \sum_{i=1}^{m} \frac{V_i}{2\pi L_i r} \tag{22}$$

where V_i and L_i are the volume and length of the nth emitted lava and m is the number of lavas that reached a distance $>r$. Notice that $h(R_{bas})$ is close to zero (as is the case $m = 1$) and for distances close enough to the vent, $h(r)$ is very similar to the value given by equation (21) (as in this case almost all lavas reached distances longer than r). As an approximation, equation (22) can be written as (In Text S1 and Figures S1 to S4 in the supporting information we show the goodness of this approximation):

$$h(r) = \alpha\left(\frac{1}{r} - \frac{r}{R_{bas}^2}\right) \tag{23}$$

where α is a constant. The second term in the parenthesis indicates that the height is 0 at $r = R_{bas}$.

Note that the topography slope Φ is (we take a positive value for slope)

$$\varphi = \tan^{-1}\left(\frac{\alpha}{r^2} + \frac{\alpha}{R_{bas}^2}\right). \tag{24}$$

Thus, for distances close enough to the vent, the edifice slope will be much greater than the repose angle, Φ_{crit}, for most earth materials. Volcano slopes rarely exceed 30°. Consequently, for distances from the vent closer than

$$r_{crit} = \sqrt{\frac{\alpha R_{bas}^2}{\tan(\varphi_{crit}) R_{bas}^2 - \alpha}}, \tag{25}$$

we impose that the volcano has a constant slope equal to Φ_{crit} and the height profile in this portion of the volcano will be

$$h(r) = (r_{crit} - r)\tan\varphi_{crit} + \alpha\left(\frac{1}{r_{crit}} - \frac{r_{crit}}{R_{bas}^2}\right) \qquad (r < r_{crit}). \tag{26}$$

Combining (25) and (26) and using $h(0) = h_{max}$:

$$r_{crit} = R_{bas}\left(\frac{\tan(\varphi_{crit}) - \sqrt{\tan^2(\varphi_{crit}) - \frac{h_{max}^2}{R_{bas}^2}}}{\tan(\varphi_{crit}) + \sqrt{\tan^2(\varphi_{crit}) - \frac{h_{max}^2}{R_{bas}^2}}}\right), \tag{27}$$

$$\alpha = \frac{R_{bas}^2}{2}\left(\tan(\varphi_{crit}) - \sqrt{\tan^2(\varphi_{crit}) - \frac{h_{max}^2}{R_{bas}^2}}\right). \tag{28}$$

The volume of the edifice is given by the volume of the solid of revolution with the profile given by equations (23) and (26):

$$V_v = \frac{\pi}{4}\left(\frac{8h_o^3 - 8\left(h_o^2 + c_1^2 R_{bas}^2\right)^{\frac{3}{2}}}{3c_1^2} + 4R_{bas}^2 h_o + \frac{8c_1 R_{bas}^3}{3}\right) + \frac{\pi r_{crit}^3 \tan(\varphi_{crit})}{3}, \tag{29}$$

with

$$h_o = \alpha\left(\frac{1}{r_{crit}} - \frac{r_{crit}}{R_{bas}^2}\right)$$

$$c_1 = \tan(\varphi_{crit}) - \sqrt{\tan^2(\varphi_{crit}) - \frac{h_{max}^2}{R_{bas}^2}}$$

In summary, we have developed a set of equations relating the properties of the plumbing system (mainly H and V_c) with the shape profile of a volcano making use of the results of magma ascent and lava erupted volumes of the previous section as follows: The depth and size of a magmatic reservoir determines the maximum height, h_{max}, and basal radius, R_{bas}, of a volcano through equations (17) and (19). R_{bas} and h_{max}, in turn, together with the critical angle Φ_{crit}, determine the edifice profile with equations (23) and (26) where parameters r_{crit} and α are defined by equations (27) and (28). The volume of the volcano is given by equation (29).

For example, Figure 2c shows the effects of H and V_c on volcano dimensions and profile. For a magmatic system with a magma density profile as shown in Figure 2a (basalt with 2% H_2O), a magma chamber of 40 km^3 and 25 km depth, a volcano will have a basal radius of ~16 km and a maximum height of ~3,000 m. The edifice volume is 262 km^3. On the other hand, a smaller magma chamber of 6 km^3 at a shallower depth of 6 km will generate a volcano with only 4 km basal radius and ~1,500 m height with a volume of only 16 km^3. These examples show that the basal radius and height will in turn control the maximum total volume that the edifice can attain via equation (29). In other words, it is possible that the spatial configuration of the plumbing system controls the maximum volume that a volcanic edifice can attain, rather than a predetermined magma budget or supply rate to the system from below.

2.3. Influence of a Deep Source

The growth of the volcano can also be affected by the magma supply rate from a deeper reservoir feeding the magma chamber (Figure 1). Pinel et al. (2010) proposed that this magma supply rate, Q_s, can be written as

$$Q_s = \frac{2a^3}{3\mu}\frac{P_s - P_c - \rho_m g(H_r - H)}{H_r - H}, \tag{30}$$

where a is the half-width of the feeder dike and μ is magma viscosity. H_r is the depth to the top of the deep reservoir (Figure 1), P_s is the pressure of the deep reservoir, and P_c is the pressure inside the magma chamber. Assuming a continuous supply rate and lithostatic pressure inside the deep reservoir, Q can be rewritten as

$$Q_s = \frac{2a^3}{3\mu}\frac{\rho_{mc} g H_r - (\rho_c g H + \Delta P) - \rho_m g(H_r - H)}{H_r - H}, \tag{31}$$

where ρ_{mc} is the mean density of the lithosphere above the deep reservoir. As the edifice grows, the erupted volume will be less, as shown previously by equation (9). This means (if the overpressure that triggers the

eruption remains the same and no viscous dissipation is considered) that after each eruption, the magma chamber will be filled with an increasing volume of extra magma compared with the previous eruption as the overpressure is not fully released. Thus, there will be a remaining overpressure (given by $\rho_m gh$, equation (9)) that will be larger after every eruption as the edifice grows. This phenomenon implies that the mean value of P_c will increase with time, reducing the magma supply rate to the magma chamber as the edifice grows. Dividing equation (31) by itself, but with the term $\rho_m gh$ incorporated into $[\rho_c gH + \Delta P]$ yields the supply rate in terms of the fraction of the initial Q_s without edifice:

$$F_{ms} = 1 - \frac{\rho_m gh}{\rho_{mc} gH_r - \rho_c gH - \rho_m g(H_r - H)}. \tag{32}$$

The supply rate to the chamber will stop when $F_{ms} = 0$, implying that the maximum height the volcano can attain under this restriction is

$$h_{\max} = \frac{\rho_{mc} H_r - \rho_c H - \rho_m (H_r - H)}{\rho_m}. \tag{33}$$

Thus $h_{\max}$ will be determined depending on which of the two conditions (equation (17) or equation (33)) gives the minimum value. Figure 2b (green line) shows that for a reservoir located at the base of the crust (40 km) the effects of the reducing supply rate of magma to the magma chamber limit the growth of a volcano. In this example, the maximum height a volcano can reach (red circles; combined restrictions of equations (17) and (33)) is 2,050 m for a magma chamber located at 19 km depth. Figure 2d shows the time it takes for a volcano to reach its maximum height using the same parameters of Figure 2c and using an initial supply rate of 0.05 km^3/yr. This plot shows that for the same initial magma supply rate, the life span of a volcano will be strongly controlled by the size and position of the magma chamber as the maximum height will be reached in a range varying from a few thousand to hundreds of thousands of years depending on these parameters. Figure 2e shows the variations of the long-term eruptive rate for the same cases analyzed in Figure 2c, according to equation (32). It shows that starting from the same initial eruptive rate, large differences occur in the eruptive rate depending again on the position of the magma chamber, with larger reductions for chambers closer to the deep reservoir. These examples show that the volume and lifetime of a volcano could be controlled by the configuration of the crustal magmatic system instead of, for example, the magma supply from the asthenosphere.

We are fully aware that we impose rather restrictive conditions on the deep magmatic source. For example, it may be the case that the overpressure relaxes by viscous flow in the time scales of interest (brittle-ductile transition or lower crust-Moho). For now we admit the simplification and postpone the examination of these conditions and its consequences to future works.

Summarizing so far, the considerations exposed in this section show how the height, basal radius, topographic profile, and morphological evolution of a volcano could be controlled by the depth of the magma chamber, crustal density structure, magma buoyancy, magma chamber overpressure, magma supply rate from a deeper reservoir, and effusion rates of eruptions. That is, the structure and dynamics of the plumbing system determine the shape and dimensions of the volcanic edifice.

3. Application to Arc Volcanoes

In this section we analyze some examples from arc volcanoes in order to apply the results and equations developed in the previous section. In section 3.1 we analyze the 1988–1990 eruption of Lonquimay volcano (Chile), together with volume estimations of ancient lava flows, to estimate plumbing system properties using the results of section 2.1. In section 3.2 we analyze the topographic profiles of some well-known volcanoes of the world with the results of section 2.2 to compare our results with previous studies. Again, we stress that the results and numbers obtained here should be seen with caution due to simplifications made and some input parameters that are poorly constrained. Still, our main aim is to assess the influence of magma chamber depth and size on volcano dimensions and morphology rather than to obtain precise values of these parameters. When possible, we compare our results with independent estimations made by previous authors of some of the parameters estimated here.

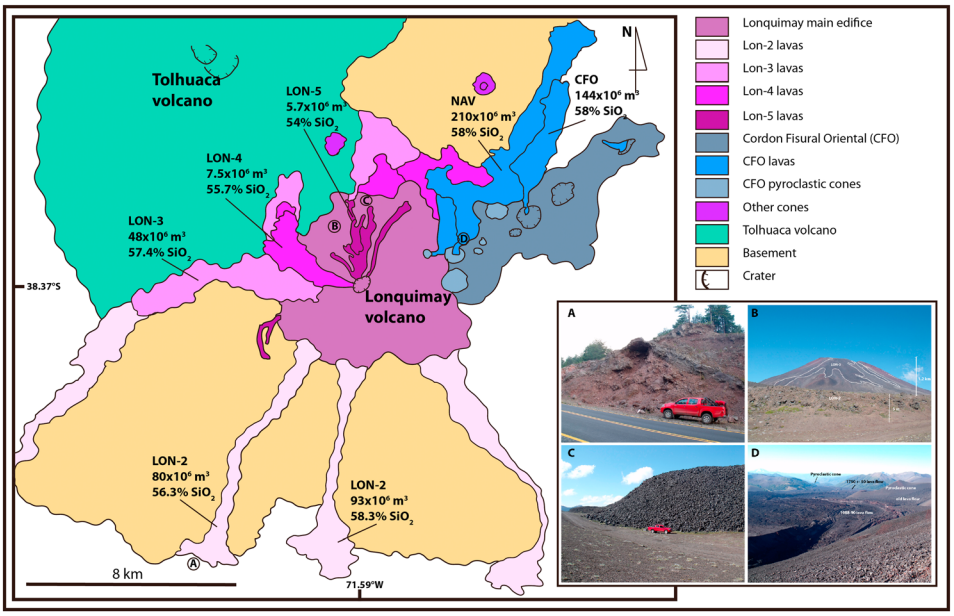

Figure 3. Geological sketch showing the Lonquimay Volcanic Complex and the lava flows units analyzed in this work. Inset shows some photographs of the main edifice and lavas of the volcano. Letters inside circles show the position of the photographs.

3.1. Case Study: Lonquimay Volcanic System

The Lonquimay Volcanic Complex (LVC) is located in the Southern Volcanic Zone of Chile (38°S; Figure 3) and has been active mainly during the Holocene. Its eruptive products range from basalts to dacites (51–65% SiO_2) with a strong prevalence (~90% vol) of basaltic andesites to andesites (54–58% SiO_2). The LVC consists of a main stratocone (MSC) with an elevation of h = 1,400 m above the local topography (measured from the lower end of older lava flows to the edifice summit) and an estimated volume of 40 km^3 (Moreno & Gardeweg, 1989) and a fissure system (Cordon Fisural Oriental, CFO) with an NE orientation and extending 10 km away from the main cone (Polanco, 2010). The CFO is formed by >10 pyroclastic cones and craters with their associated lavas (Figure 3). Most of the products that build the MSC and CFO are lavas, but products of explosive eruptions (mainly fall and pyroclastic flow deposits) outcrop to the east of the LVC extending to >25 km from the vents (Gilbert et al., 2014). While recognized pyroclastic deposits are younger than 11,800 years (Gilbert et al., 2014), age dating on lava flows has been much more difficult with few reliable ages (Moreno & Gardeweg, 1989) and the relative ages of flows were established using mainly stratigraphic and morphological criteria.

The MSC is divided into five lava units ranging from late Pleistocene to the present (Lon-1 to Lon-5, Moreno and Gardeweg (1989); Figure 3). Lon-1 lavas have a very limited exposure as isolated outcrops as they are mostly covered by younger units. Lava flows from Lon-2 reach up to 12 km from the vent and are strongly confined inside deep valleys. Morphologically, they are mainly 'a' a flows (Figure 3a). On the other hand, lava flows from Lon-5 unit are only up to 3 km in length with a blocky morphology (Figures 3b and 3c), although the composition is roughly the same for all units.

The CFO is the zone where most of the historic activity of the LVC has taken place (last eruptions in 1988–1990, 1887–1889 and 1853). Lava flows are up to 10 km in length, with compositions ranging from andesite to dacite (56–65% SiO_2) and with a blocky morphology (Figure 3d).

Petrographically, all the analyzed lavas are very similar. The mineral assemblage for most samples consists of plagioclase, clinopyroxene, and olivine, with subordinate orthopyroxene and Fe-Ti oxides. The dominant texture of the rocks is aphiric (<2–3% phenocrysts), and crystal contents (phenocrysts and microphenocrysts) are very uniform.

We analyzed some of the best exposed lavas of the LVC in order to estimate their volume, glass, and mineral composition and calculate their effusion rates (Figure 4). Figure 4a shows a progressive shortening from

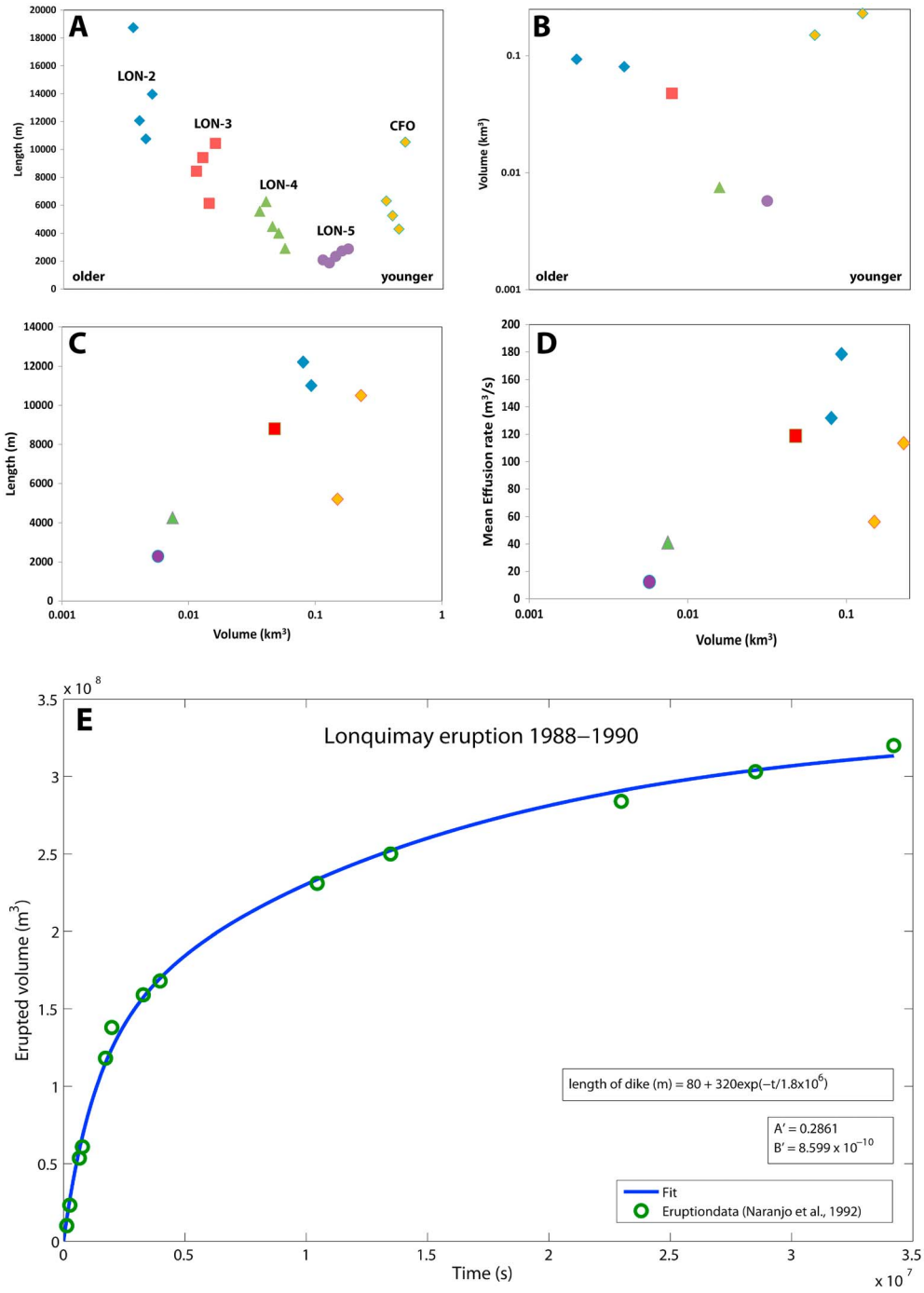

Figure 4. (a) Measured maximum length for lava flows from LVC. (b) Volume of selected lava flows versus approximate time of eruption. (c) Maximum length versus volume for the same lavas from Figure 4b. (d) Mean effusion rate versus volume for the same lava flows from Figure 4b. (e) Erupted volume versus time from the 1988–1990 Navidad eruption at the LVC. The solid line is the best fit of the data using equation (4), varying the parameters *A* and *B*.

unit Lon-2 to Lon-5 in the maximum lengths of lavas of the MSC. We measured the volumes of lava flows by measuring its thicknesses at several points, calculating the average value, and multiplying it by the surface area. The volumes of the erupted lavas (Figure 4b) show a progressive reduction, from ~0.1 km^3 for unit Lon-2 to 0.006 km^3 for unit Lon-5. On the other hand, lavas from the CFO represent a shift to larger erupted volumes, and they correspond to the largest lavas that can be measured from the entire

volcanic complex, with a maximum of 0.23 km^3 (lava flow from 1988 to 1990 eruption). It is important to note that the estimated volume of the lavas represents a minimum, especially the older ones, as they usually are covered by younger lavas in areas close to the vent and we cannot estimate volumes for LON-1 lavas.

We were not able to measure the volume of all the lavas depicted in Figure 4a, as most lavas are partially covered by younger flows, pyroclastic deposits, or vegetation. Still, we believe that the volume trend shown in Figure 4b is valid for the entire evolution of the volcanic complex, as there is a very good correlation between maximum length and volume, except for lavas from the CFO (which will be discussed later, Figure 4c).

The mean effusion rates of the analyzed lava flows were estimated using the method proposed by Castruccio et al. (2014) for cooling-limited flows. Our results indicate a decreasing trend with age and again a strong correlation with erupted volume (with the exception of the CFO lavas; Figure 4d.) with maximum values from 170 m^3/s for Lon-2 lavas to less than 10 m^3/s for unit Lon-5. It is important to note that effusion rate estimates are independent of volume measurements as they are calculated using thickness, slope, and viscosity estimates, rather than total volume (Castruccio et al., 2014; Castruccio & Contreras, 2016).

We suggest that as the cone was growing, the driving pressure that makes the magma ascend decreased, with a progressive reduction of the effusion rates and erupted volumes during eruptions from LON-2 to LON-5. The edifice grew up to the point when the system was no longer able to erupt through the volcano summit. Then, as magma continued to accumulate into the reservoir, the overpressure continued to build up until magma found a new path of less resistance to the surface through the NE lineament, starting lateral eruptions not affected by the volcano height, building the CFO, and having similar volumes and effusion rates to those associated with the first stages of the volcano.

3.1.1. Estimations of Plumbing System Parameters

Here we used data from the last eruption of Lonquimay volcano (1988–1990), together with volcano dimensions, volume estimates of lavas erupted through the evolution of the volcano, geothermobarometry, and previously published seismicity data to estimate some of the magmatic system parameters of the volcano.

We believe that the volcano is very close to its maximum height as the ratio between volumes of the youngest and oldest lavas is very low ($\sim 2 \times 10^{-2}$) and all historical eruptions have occurred in the CFO. According to equation (17) and using $\Delta P_i = 25$ MPa, the chamber feeding eruptions should be located at a depth of ~6 km below the base of the edifice.

We made an independent estimation of the storage depth applying the clinopyroxene-glass geothermobarometer (Putirka, 2008) on selected samples from the 1988 to 1990 eruption. The chemical compositions of glass and minerals used in the calculations are presented in Text S2 and Tables S3 to S10. A sample from the base of the fall deposit gave a depth range of 4.6–11.8 km, and a sample from the top of the deposit gave a range between 7.3 and 13.5 km. The average of the minimum depth values (assuming that it represents the top of the magma chamber) of both measurements gave a value of H = 6 km, which we used for the subsequent calculations. This value is in very good accordance with the estimation made by Barrientos and Acevedo-Aránguiz (1992), who estimated the magma chamber to be localized 6–10 km below the surface based on the location of hypocenters of seismic events during the 1988–1990 eruption.

For the 1988–1990 eruption we take h = 0 as it occurred in the CFO. This eruption was studied in detail by Moreno and Gardeweg (1989) and Naranjo et al. (1992). This mainly strombolian eruption lasted 13 months, emitting 0.32 km^3 (DRE; Figure 4e) of andesitic magma (58% wt SiO_2), generating a 10 km long lava flow and a 200 m high pyroclastic cone in the NE flank of the main edifice. Figure 4e shows the erupted volume versus time for this eruption taken from Naranjo et al. (1992). According to Stasiuk et al. (1993), the conduit dimensions varied from a 400 m × 5 m fissure at the beginning of the eruption to 80 m × 5 m at the end. The same authors suggested that the conduit dimensions were stabilized after the first 100 days of the eruption. We estimated the viscosity of the magma analyzing tephra samples from different stages of the eruption, using its glass composition and crystal content (Castruccio et al., 2010). The parameters used in the modeling are listed in Tables S1 and S2. The calculations suggest that the viscosity remained fairly constant through the

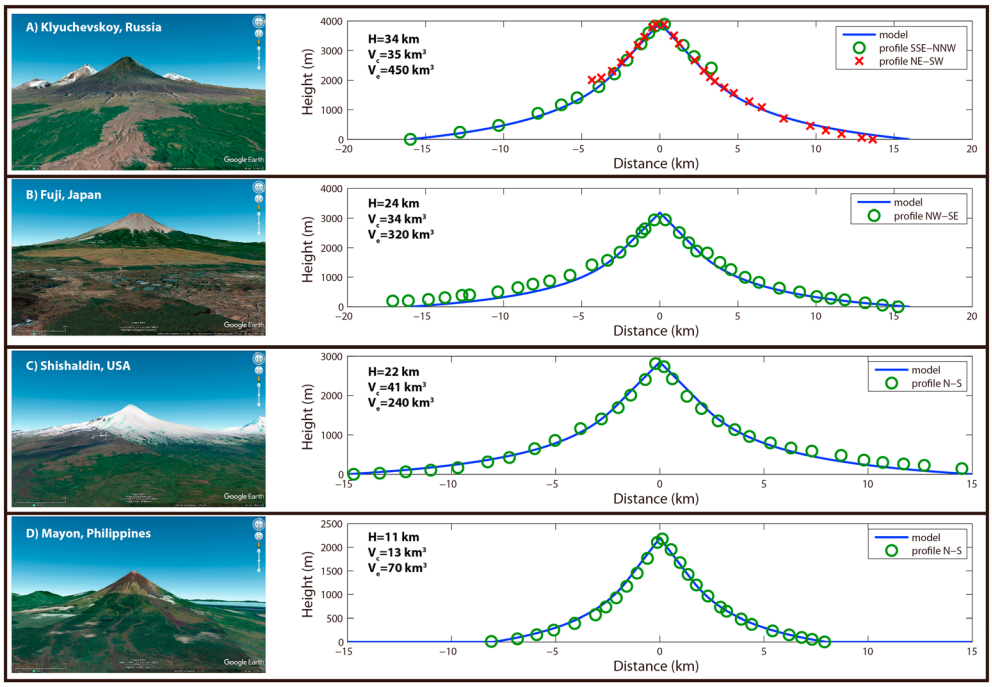

Figure 5. Volcano topographic profiles for (a)Klyuchevskoy, Russia; (b) Fuji, Japan; (c) Shishaldin, USA; and (d) Mayon, Philippines. Each figure indicates the parameters H and V_c used in the fit and the total resulting volume of the volcano.

eruption with a value of ~1.5×10^5 Pa s. To account for the variations of dike length, we modified equation (4), replacing l with

$$l = 80 + 320 \exp\left(\frac{-t}{1.8\times10^6}\right). \tag{34}$$

In this case equation (4) can be solved only numerically (we replaced A and B by A′ and B′ respectively, where A′ = A/l and B′ = B/l). We fitted the data from Figure 4e with values of A′ = 0.286 m^2 s^{-1} and B′ = 8.6 x 10^{-10} m^{-1} s^{-1}. With equation (6), we estimated a volume of ~49 km^3 for the magma chamber. We used equation (15) to estimate the dike width w, obtaining a value of ~4 m.

3.2. Other Examples From Arc Volcanoes

In the following examples we fitted the topographic profiles of selected volcanoes to estimate the size and depth of the magma chamber. We defined the base of a volcano as the average level reached by the longest lava flows of a volcano. The basal radius was defined as the mean distance from the vent reached by these flows. The estimated volcano volumes in our calculations are somewhat larger than previous measurements (e.g., Grosse et al., 2014) as we assume a flat base without considering previous topography. We are assuming that the analyzed volcanoes reached their maximum heights; thus, our estimates should be considered as minimum values. In all the examples we set $\phi_{crit} = 30°$, $\Delta P_i = 25$ MPa and a H_2O content of 2%. Magma compositions are listed in supporting information.

Klyuchevskoy volcano is the largest volcano of the Kamchatka peninsula and is part of the Klyuchevskaia Volcanic Group (Fedotov et al., 2010). It is one of the tallest subduction volcanoes in the world, with an ~3,500–4,000 m height from its base. According to equation (17), the magma chamber that feeds eruptions should be deep enough for buoyancy forces to be sufficiently high to build the volcano. We estimated the depth and size of the magma chamber of this volcano by fitting its topographic profile with equations (23) and (26) (Figure 5a). Using $\kappa' = 10^{10}$ Pa and $\Delta P_i = 25$ MPa, together with magma and crust density profiles (see the supporting information: density profile constructed with magma composition of Table S11 and density profile as shown in Table S12) we obtained $H = 34$ km and $V_c = 35$ km^3. The results compare well with the actual topography. Fedotov et al. (2010) estimated that the volcanic system has two main reservoirs located at 0–5 and 25–40 km depth. Their seismic data indicate that before the beginning of eruptions,

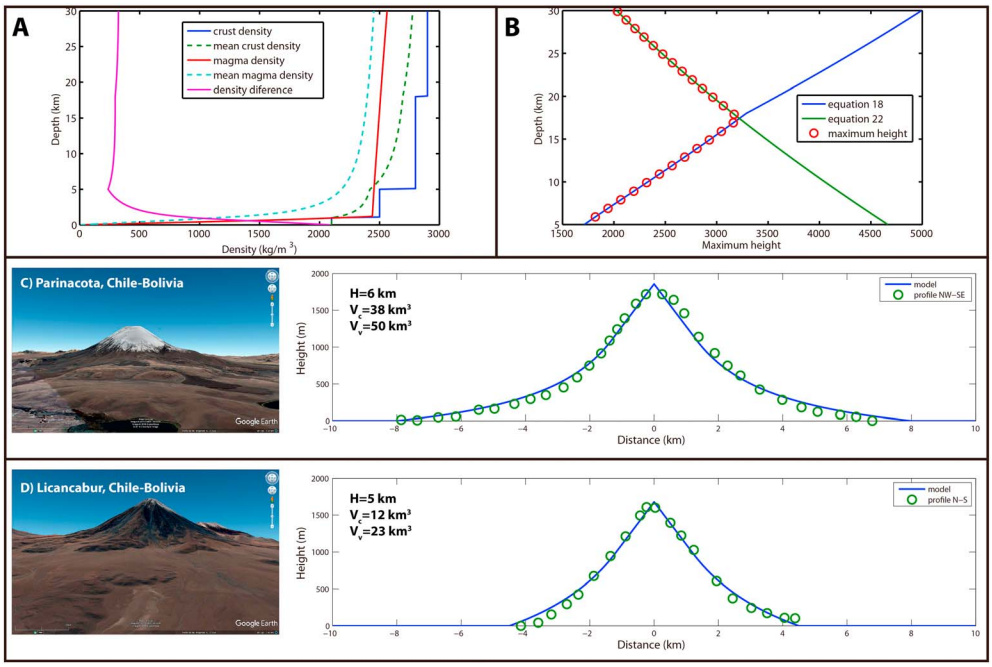

Figure 6. (a) Crustal and magma density profiles (and their mean values) with depth for Unzen volcano. Also shown is the difference between the mean values of magma and crust density. (b) Maximum height that a volcano can attain according to equations (17) and (21) and using the parameters of Figure 6a. (c) Volcano topographic profile for Parinacota volcano, Chile-Bolivia. (d) Volcano topographic profile for Licancabur volcano, Chile-Bolivia.

seismicity starts at deep locations (30–40 km) in the days to months before the eruption and migrates upward as the eruption proceeds. Our results support the idea of a deep source for eruptions at this volcano, although magma can be temporarily stored at shallow depths as shown by Koulakov et al. (2013).

Fuji volcano is the highest mountain in Japan (3,776 m above sea level (asl)), and its summit is located 3,200 m above its base. Using a typical composition for lavas of the volcano (Ishibashi, 2009; see Table S11 in the supporting information) and its topographic profile (Figure 5b), we found that the magma chamber that feeds the volcano should be at ~24 km depth and V_c = 34 km^3. Seismic tomography results (Kaneko et al., 2010) indicate at least two reservoirs located at 8–9 and >20 km depth.

Figures 5c and 5d show topographic profiles for Shishaldin (Alaska, USA) and Mayon (Philippines) volcanoes. Both volcanoes can be fitted with H = 22 and 11 km and V_c = 41 km^3 and 13 km^3, respectively. It is interesting to note that no surface deformation has been detected before eruptions at both volcanoes and this has been attributed to deep magma chambers feeding their eruptions (Jentzsch et al., 2001; Moran et al., 2006).

It is also interesting to note that all these examples correspond to volcanoes with mainly basaltic products, which should be smaller than more silicic volcanoes based on their lower density (based on equation (17)). A counterexample to this trend is Mount Shasta (USA) in the Cascades range with a height of 3,200 m above its base. This volcano is composed mainly by dacitic lavas. According to the density profile of a typical magma from this volcano (taken from Grove et al., 2005) and the crust profile (Fuis et al., 1987), the magma chamber should be located at 19 km. Grove et al. (2005) proposed at least three reservoirs for Mount Shasta at 3–6, 7–10, and 15–25 km depth.

Mount Unzen (Japan) is a volcano with a height of 1,486 m asl and its last activity was between 1990 and 1995. According to the density profile of its magma (Figure 6a; using a magma composition from Nakamura, 1995) the magma chamber should be located at <5 km below the surface (Figure 6b). Ohmi and Lees (1995) argued that Unzen plumbing system is composed of two chambers at 2.5–5 and 7.5–12.5 km. It is noteworthy that preeruption seismicity of the 1990–1995 cycle started in 1989 at 15 km depth and migrated slowly to shallower depths of 5 km, 1 month before the eruption. This would be indicating a slower ascent of magma compared with basaltic volcanoes such as Klyuchevskoy, and thus, the source pressure of the eruption was the shallower chamber as it was probably hydraulically isolated from deeper

chambers. A similar result can be obtained from Soufriere Hills volcano. We did not draw topographic profiles of these volcanoes as they are strongly controlled by preexisting topography and are constructed by a high proportion of lava domes with an irregular profile.

The Central Volcanic Zone of northern Chile and Bolivia exhibits a high concentration of andesitic-dacitic composite volcanoes (González, 1995). These volcanoes are usually <1,800 m above their bases with basal radii <10 km (González, 1995). We fitted the profiles of two of the most symmetrical cones (Parinacota and Licancabur; Figures 6c and 6d), and our results indicate shallow reservoirs (5–6 km depth) in accordance with petrological studies (e.g., Feeley & Davidson, 1994; Matthews et al., 1999) that pointed out storage regions <10 km depth for volcanoes of this region.

4. Discussion

In this study we presented a physical modeling exercise involving magma ascent, extruded volumes of lavas, and volcano topographic profile that relates characteristic parameters of a plumbing system, such as depth and size of the reservoir, with parameters directly measurable at the surface. A key finding was that the spatial distribution of the central elements of the plumbing system controls the total volume of the edifice (height and maximum radius), rather than a preeruptive magma budget or magma influx rate.

Our approach was restricted only to effusive eruptions. However, we are aware that magma ascent in a conduit during explosive eruptions is more complex due to fragmentation, the increased role of volatile exsolution, turbulence, and high exit velocities. We recognize that it would be interesting to incorporate these mechanisms in a more general model to analyze the complete history of a volcano, including explosive and effusive eruptions, but it is beyond the scope of this work, and according to Davidson and De Silva (2000), the cone-building association of volcano edifices is composed mainly by lava flows. Nevertheless, we believe that our approximation of considering the 1988–1990 Lonquimay eruption as mainly effusive yielded reasonable results employing our model.

In our model, we conceived the magmatic reservoir as a single body filled homogeneously with magma and connected to the surface by a single conduit with spatially constant dimensions. We were also assuming a constant effective bulk modulus for the magma inside the magma chamber. As mentioned by Mastin et al. (2008), the complexity of partially molten bodies is much greater than that accounted for in our model, and perhaps many of the simplifications made here could be considered as too unrealistic.

We believe, however, that the theoretical relationships given in this work can offer some insights into the role that the depth and size of a magmatic reservoir plays in the construction process of a volcano. We discuss in the following sections some of the implications of our work.

4.1. The Influence of Plumbing System on Volcano Dimensions

We found that volcanoes fed by deep (>20 km) magma chambers are taller than volcanoes associated with shallower systems. Our analysis also supports the hypothesis that the depth and size of the magma chamber influence the edifice volume and magma supply rate. It is clear from studies of the last decades that plumbing systems associated with volcanoes are complex and with multiple reservoirs located at different depths (e.g., St Helens, Etna; Cashman et al., 2017), thus apparently invalidating the practical application of our model. However, we identified some patterns that can help to better understand the nature of these complex systems.

Many of the tallest subduction volcanoes have products of basaltic composition, and our results indicate that these volcanoes are fed by sources located at >20 km depth. Koulakov et al. (2013) identified a permanent magma source at >30 km depth under Klyushevskoy volcano and transient storage regions at 10–12 km and <5 km during eruptive episodes between 1999 and 2009. The time interval between the onset of seismicity at depth and the start of a new eruptive cycle is usually weeks or a couple of months. On the other hand, volcanic systems with more evolved magma compositions such as Soufriere Hills and Unzen also show evidence of multiple storage regions at different depths, but the onset of seismicity and migration of magma takes much longer (>1 year) before the start of the eruption (White & McCausland, 2016).

We propose that systems composed mainly by basaltic magma build volcanoes with the potential to reach >2,500 m above its base as the low viscosity of the magma allows it to ascend through the crust very fast

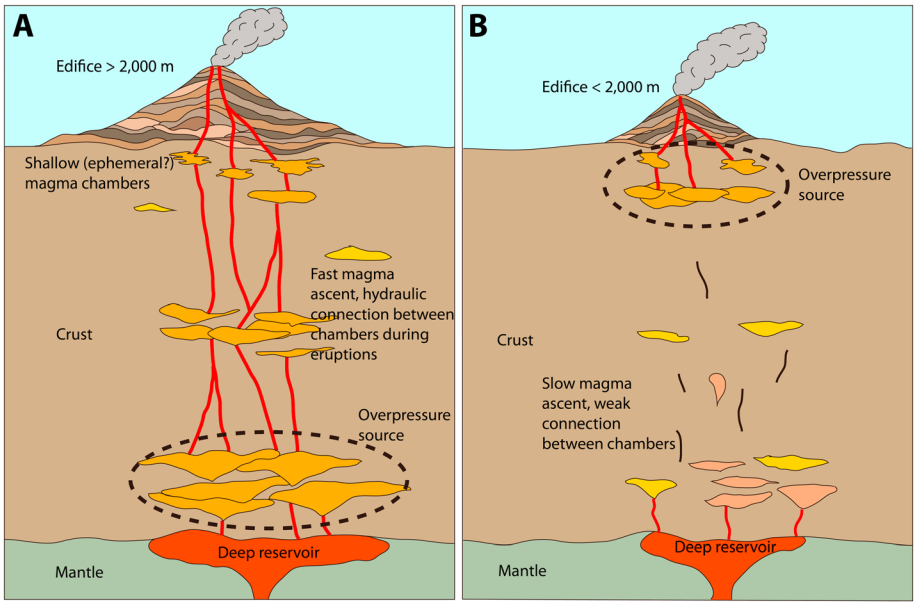

Figure 7. Cartoon that hypothesizes the main differences in the plumbing system of different types of volcanoes. (a) For volcanoes with heights >2,000 m and base radius > 10 km, eruptions are fed by a deep magma chamber that is well connected with shallow chambers. Magma could be stored by short periods of time on these shallow chambers, but the overpressure driving the eruption is generated in the deep chamber. (b) For volcanoes with heights <2,000 m and base radius <10 km, eruptions are feed by a shallow magma chamber that is fed sporadically by deeper reservoirs, without a permanent hydraulic connection.

from deep magma chambers. In these volcanoes intermediate chambers exist, but these storage regions are ephemeral and are continuously connected during the eruptive cycle and the ultimate pressure source of the eruption is the deep magma chamber (Figure 7a). This hydraulic connection between deep and shallow reservoirs during eruptions has been recently suggested by Shapiro et al. (2017) by analyzing seismic data at the Klyuchevskoy volcanic group. In more silicic magma systems, magma ascent is slower and more difficult. In this scenario, different storage regions are not continuously connected during eruptions, and the eruptive source pressure is the shallow magma chamber (Figure 7b). In a couple of recent works (Cashman et al., 2017; Sparks & Cashman, 2017), the concept of transcrustal magmatic systems has been proposed, in which the shallow magma chamber (1–10 km depth) of a volcano represents only a small fraction of the entire magmatic system, which embraces the whole crust. In this framework, and considering that our results indicate a wide range of chamber depths (~5–30 km) for different volcanoes, our method can help to identify the depth at which the overpressure that triggers an eruption is generated inside the larger system.

As mentioned by Wilson et al. (1992), volcano height is not only related to magma source depth (although here we relate the height of the volcano with magma chamber depth, not source depth), but to a number of other factors such as magma supply rate, eruption frequency, and erupted volumes. Interestingly, the physical relationships derived in this work indicate that depth and size of the magma chamber control basal radius and maximum height of a volcano. These parameters control the maximum volume that the edifice can reach, which in turn will influence the lifetime of the volcano. Further implications can be investigated in future works. For example, equation (33) implies that under certain circumstances, when the magma chamber is very close to the feeding deeper reservoir, maximum volcano height is close to zero. It is widely proposed (e.g., Morgado et al., 2015; Walker, 2000) that many monogenetic cones and fields are fed by deep sources from the crust-mantle region, without intermediate reservoirs. Our results suggest a possible mechanism that can inhibit the growth of a large stratocone under these conditions. Such a mechanism (see section 2.3) entails an extra overpressure in the magma chamber. However, we ignore other potentially important mechanisms of overpressure release besides eruption, such as viscous deformation and earthquake faulting of the host rocks. Hence, the study of this proposed mechanism should warrant a careful discussion of host rheology as a function of depth and its role on the time evolution of overpressure during volcano growth.

Finally, another implication that can be extracted from Figures 2c and 2d is that large and long initial lava flows promote larger volcano volumes and consequently a long period of volcano growth. This can explain the longer period of life of some shield volcanoes compared with conical stratocones. It is out of the scope of

this work to investigate the details of these implications, but we believe that further thought about them is worthwhile.

4.2. Interpretation of Topographic Profiles of Arc Volcanoes

In section 2.2 we developed a series of equations for the volcano shape profile as a function of magma physical properties and location and size of magma chamber. The equations are based on the simple principle that the thickness of a pile of material distributed radially from a single source decreases with distance from the source as the planimetric area to cover increases and is proportional to the perimeter of a circle with radius equal to the distance from the vent. This model is valid for simple cones with a single source and a flat base. The surprisingly good fit of our model with many volcanoes suggests that this basic relationship is valid not only for the stacking of lava flows from a vent but probably also for other types of flows such as pyroclastic density currents and lahars that also represent an important part of the total volume of most volcanoes.

Most works on volcano morphology have been focused mostly on morphometric analyses (e.g., Grosse et al., 2014; Karatson et al., 2010; Wood, 1978; Wright et al., 2006), but a few have suggested mechanisms of growth to explain the profiles of volcanoes. Borgia and Linneman (1992) applied a model of growth to Arenal volcano. They noticed that lava flows were shorter on steeper slopes (although we believe that this is due to the fact that steeper slopes are commonly associated with higher altitudes and lavas emitted from higher vents produce shorter flows), and they modeled the volcano profile with a relationship of the form $h(r) = \ln(1/r + \text{constant})$ for distal areas and a constant slope when the slope is above a critical angle in the proximity of the vent. A logarithmic profile for distal parts of volcanoes has also been proposed by Karatson et al. (2010). We believe that the good fit of both models to volcano profiles ($h \sim 1/r$ and $h \sim \ln(1/r)$) is due to the fact that both models use a constant slope in proximal areas, and for large enough r, both functions are similar ($\ln[1/r + 1] \rightarrow 1/r$ for large r). Karatson et al. (2010) classified volcanoes in two types depending on the slope of the upper part of the cone, relating more concave profiles to effusive-dominant volcanoes and more constant slopes to slightly more explosive-dominant volcanoes. Davidson and De Silva (2000) also classified volcanoes into two types, identifying primary cones with constant slopes and equilibrium concave profiles for mature volcanoes where mass wasting processes are important. According to our results, the different types of volcanoes described by these authors can be modeled with the same set of equations (equations (23) and (26)). We believe that the differences observed can be explained as follows: for volcanoes with small basal radii the mean slope of the edifice is larger for a given volcano height and closer to ϕ_{crit}, and they appear to be more like simple straight-flanked cones (for example, Licancabur and Parinacota volcanoes in Figures 6c and 6d). In any case, our topographic profile model should be interpreted as a starting point for future works that could incorporate migration of multiple vents, fallout deposits, previous topography, and erosion processes.

Previous authors have proposed that the maximum height of a volcano is (among other parameters) a function of the emitted volume. Our results show that the volume erupted by a volcano is a function of the maximum height it can attain and the length of the largest lavas emitted, which in turn is controlled by the lava volume. Detailed chronological and volcano evolution studies (e.g., Clavero et al., 2004; Conway et al., 2016; Hildreth & Lanphere, 1994) show evidence that volcano activity occurs in pulses or cycles of peak activity followed by more quiet stages. Although the model presented here uses a continuous supply of magma and consequently a regular pattern of eruption frequency, it captures the observation that the cone building can be very fast. In fact, model results (Figure 2d) indicate that ~90% of the edifice can be constructed in $<$10–100 kyr in agreement with volcano evolution studies (Davidson & De Silva, 2000).

5. Conclusions

Our main conclusions can be summarized as follows:

1. The vertical structure and connectivity of the plumbing system determine the shape and dimensions of the volcanic edifice. According to our hypothesis, plumbing system properties, such as depth and reservoir volume, determine effusion rates and volumes of lava flows. Their decay in time between eruptions, as exhibited by many arc volcanoes, could be due to the increase in vent elevation as the volcano grows. Thus, we can constrain properties of the plumbing system such as chamber depth and size, and conduit dimensions, by measuring commonly accessible observables for volcanologists like eruption rates and lava flow dimensions.

2. Under appropriate conditions and assumptions such as an intermediate to deep magma reservoir (>5 km depth) and a predominance of effusive activity, the dimensions of a simple volcanic cone resulting from the emission of lava flows can be interpreted as the interplay of the plumbing system parameters mentioned above. Large volcanoes (height > 2,000 m; basal radius > 12 km; and volume > 100 km^3) are related to basaltic systems with intermediate to deep and large magma chambers where buoyancy effects become noticeable. Small volcanoes (height < 1,800 m; basal radius < 7 km; and volume < 50 km^3) are related to more evolved systems with shallow magma chambers as pressure sources of eruptions, with little buoyancy effects. Consequently, volcano dimensions can be interpreted as indicators of key properties of the plumbing system.
3. Topographic profiles of arc volcanoes can be modeled essentially as a pile of lavas that are reducing their dimensions with time and which are emitted from a point source. The topographic profile model developed here can be applied to different types of single-vent arc volcanoes that previous studies attributed to different eruptive mechanisms and mass-wasting processes.
4. Due to the high complexity of plumbing systems in terms of their multiple levels of magma storage and their relative importance on volcano activity, it is best to combine our approach with geophysical and petrologic observations to unravel the true nature of reservoirs and their role during eruptions that build volcanic edifices.

Acknowledgments
This study was funded by FONDECYT project 11121298 and FONDAP project 15090013. CONAF is thanked for access permission to protected areas. We thank the reviews of L. Wilson and an anonymous reviewer that greatly improved the final version of this work. Data used are listed in references and in the supporting information. MATLAB codes used for calculations and topographic profiles are available upon request to the corresponding author.

References

Alfano, F., Bonadonna, C., Volentik, A., Conno, C., Watt, S., Pyle, D., & Connor, L. (2011). Tephra stratigraphy and eruptive volume of the May, 2008, Chaitén eruption, Chile. *Bulletin of Volcanology*, *73*(5), 613–630. https://doi.org/10.1007/s00445-010-0428-x

Annen, C., Lénat, J.-F., & Provost, A. (2001). The long-term growth of volcanic edifices: Numerical modeling of the role of dyke intrusion and lava-flow emplacement. *Journal of Volcanology and Geothermal Research*, *105*(4), 263–289. https://doi.org/10.1016/S0377-0273(00)00257-2

Barrientos, S., & Acevedo-Aránguiz, P. (1992). Seismological aspects of the 1988–1989 Lonquimay (Chile) volcanic eruption. *Journal of Volcanology and Geothermal Research*, *53*(1-4), 73–87. https://doi.org/10.1016/0377-0273(92)90075-O

Ben-Avraham, Z., & Nur, A. (1980). The elevation of volcanoes and their edifice heights at subduction zones. *Journal of Geophysical Research*, *85*(B8), 4325–4335. https://doi.org/10.1029/JB085iB08p04325

Blake, S. (1981). Volcanism and the dynamics of open magma chambers. *Nature*, *289*(5800), 783–785. https://doi.org/10.1038/289783a0

Blake, S. (1984). Volatile oversaturation during the evolution of silicic magma chambers as an eruption trigger. *Journal of Geophysical Research*, *89*(B10), 8237–8244.

Bonadonna, C., Pistolesi, M., Cioni, R., Degruyter, W., Elissondo, M., & Baumann, V. (2015). Dynamics of wind-affected volcanic plumes: The example of the 2011 Cordón Caulle eruption, Chile. *Journal of Geophysical Research: Solid Earth*, *120*, 2242–2261. https://doi.org/10.1002/2014JB011478

Borgia, A., & Linneman, S. (1992). On the mechanisms of lava flow emplacement and volcano growth: Arenal, Costa Rica. In J. H. Fink (Ed.), *Lava Flows and Domes: Emplacement Mechanisms and Hazard Implications* (pp. 208–243). Berlin: Springer-Verlag.

Branca, S., De Beni, E., & Proietti, C. (2013). The large and destructive 1669 AD eruption at Etna volcano: Reconstruction of the lava flow field evolution and effusion rate trend. *Bulletin of Volcanology*, *75*(2), 694. https://doi.org/10.1007/s00445-013-0694-5

Carey, S., & Sparks, R. S. J. (1986). Quatitative models of the fallout and dispersal of tephra from volcanic eruptions columns. *Bulletin of Volcanology*, *48*(2-3), 109–125. https://doi.org/10.1007/BF01046546

Carrasco-Nuñez, G. (1997). Lava flow growth inferred from morphometric parameters: A case study of Citlatépetl volcano, Mexico. *Geological Magazine*, *134*(2), 151–162. https://doi.org/10.1017/S0016756897006614

Cashman, K. V., Sparks, R. S. J., & Blundy, J. D. (2017). Vertically extensive and unstable magmatic systems: A unified view of igneous processes. *Science*, *355*(6331), eaag3055. https://doi.org/10.1126/science.aag3055

Castillo, P. R., & Newhall, C. G. (2004). Geochemical constrains on possible subduction components in lavas of MAyon and Taal volcanoes, Southern Luzon, Philippines. *Journal of Petrology*, *45*(6), 1089–1108. https://doi.org/10.1093/petrology/egh005

Castruccio, A., & Contreras, M. (2016). The influence of effusion rate and rheology on lava flow dynamics and morphology: A case study from the 1971 and 1988–1990 eruptions at Villarrica and Lonquimay volcanoes, Southern Andes of Chile. *Journal of Volcanology and Geothermal Research*, *327*, 469–483. https://doi.org/10.1016/j.jvolgeores.2016.09.015

Castruccio, A., Rust, A. C., & Sparks, R. S. J. (2010). Rheology and flow of crystal-bearing lavas: Insights from analogue gravity currents. *Earth and Planetary Science Letters*, *297*(3-4), 471–480. https://doi.org/10.1016/j.epsl.2010.06.051

Castruccio, A., Rust, A. C., & Sparks, R. S. J. (2014). Assessing lava flow evolution from post-eruption field data using Herschel-Bulkley rheology. *Journal of Volcanology and Geothermal Research*, *275*, 71–84. https://doi.org/10.1016/j.jvolgeores.2014.02.004

Clavero, J., Sparks, R. S. J., Polanco, E., & Pringle, M. (2004). Evolution of Parinacota volcano, Central Andes, Northern Chile. *Revista Geologica de Chile*, *31*(2), 317–347.

Conway, C. E., Leonard, G. S., Townsend, D. B., Calvert, A. T., Wilson, C. J. N., Gamble, J. A., & Eaves, S. R. (2016). A high-resolution $^{40}Ar/^{39}Ar$ lava chronology and edifice construction history for Ruapehu volcano. *Journal of Volcanology and Geothermal Research*, *327*, 152–179. https://doi.org/10.1016/j.jvolgeores.2016.07.006

Daniels, K., Kavanagh, J., Menand, T., & Sparks, R. S. J. (2012). The shapes of dykes: Evidence for the influence of cooling and inelastic deformation. *GSA Bulletin*, *124*(7-8), 1102–1112. https://doi.org/10.1130/B30537.1

Davidson, J., & De Silva, S. (2000). Composite volcanoes. In H. Sigurdsson (Ed.), *Encyclopedia of Volcanoes* (pp. 663–681). San Diego, CA: Academic Press.

Deardoff, N., & Cashman, K. V. (2012). Emplacement conditions of the c. 1600-year BP Collier Cone lava flow, Oregon: A LiDAR investigation. *Bulletin of Volcanology*, *74*(9), 2051–2066. https://doi.org/10.1007/s00445-012-0650-9

Epp, D., Decker, R., & Okamura, A. (1983). Relation of summit deformation to East Rift Zone eruptions on Kilauea volcano, Hawaii. *Geophysical Research Letters*, *10*(7), 493–496. https://doi.org/10.1029/GL010i007p00493

Fedotov, S. A., & Zharinov, N. A. (2007). On the eruptions, deformation, and seismicity of Klyuchevskoy Volcano, Kamchatka in 1986–2005 and the mechanisms of its activity. *Journal of Volcanology and Seismology*, *1*(2), 71–97. https://doi.org/10.1134/S0742046307020017

Fedotov, S. A., Zharinov, N. A., & Gontovaya, L. I. (2010). The magmatic system of the Klyuchevskaya group of volcanoes inferred from data on its eruptions, earthquakes, deformation and deep structure. *Journal of Volcanology and Seismology*, *4*(1), 1–33. https://doi.org/10.1134/S074204631001001X

Feeley, T., & Davidson, J. (1994). Petrology of calc-alkaline lavas at volcan Ollague and the origin of compositional diversity at Central Andean stratovolcanoes. *Journal of Petrology*, *35*(5), 1295–1340. https://doi.org/10.1093/petrology/35.5.1295

Figueroa, O., Deruelle, B., & Demaiffe, D. (2009). Genesis of adakite-like lavas of Licancabur volcano (Chile-Bolivia, Central Andes). *Comptes Rendus Geoscience*, *341*(4), 310–318. https://doi.org/10.1016/j.crte.2008.11.008

Fuis, G., Zucca, J., Mooney, W., & Milkereit, B. (1987). A geological interpretation of seismic-refraction results in northeastern California. *GSA Bulletin*, *98*(1), 53–65. https://doi.org/10.1130/0016-7606(1987)98%3C53:AGIOSR%3E2.0.CO;2

Gilbert, D., Freundt, A., Kutterolf, S., & Burkert, C. (2014). Post-glacial time series of explosive eruptions and associated changes in the magma plumbing system of Lonquimay volcano, south central Chile. *International Journal of Earth Sciences*, *103*(7), 2043–2062. https://doi.org/10.1007/s00531-012-0796-x

Giordano, D., Russell, J. K., & Dingwell, D. B. (2008). Viscosity of magmatic liquids: A model. *Earth and Planetary Science Letters*, *271*(1-4), 123–134. https://doi.org/10.1016/j.epsl.2008.03.038

González, O. (1995). Volcanes de Chile. Instituto Geográfico Militar, Santiago (in spanish). 635 pp.

Grosse, P., Euillades, P., Euillades, L., & Van Wyk de Vries, B. (2014). A global database of composite volcano morphometry. *Bulletin of Volcanology*, *76*(1), 784. https://doi.org/10.1007/s00445-013-0784-4

Grove, T., Baker, M., Price, R., Parman, S., Elkins-Tanton, L., Chatterjee, N., & Muntener, O. (2005). Magnesian andesite and dacite lavas from Mt. Shasta, northern California: Products of fractional crystallization of H2O-rich mantle melts. *Contributions to Mineralogy and Petrology*, *148*(5), 542–565. https://doi.org/10.1007/s00410-004-0619-6

Gudmundsson, A. (2006). How local stresses control magma-chamber ruptures, dyke injections, and eruptions in composite volcanoes. *Earth-Science Reviews*, *79*(1-2), 1–31. https://doi.org/10.1016/j.earscirev.2006.06.006

Harris, A. J. L., & Rowland, S. K. (2009). Effusion rate controls on lava flow length and the role of heat loss: A review. In T. Thordarson et al. (Eds.), *Studies in Volcanology. The Legacy of George Walker*, *Special Publications of IAVCEI*, (pp. 33–51). London: Geological Society.

Hildreth, W., & Lanphere, M. A. (1994). Potassium-argon geochronology of a basalt-andesite-dacite arc system: The Mount Adams volcanic field, Cascade Range of southern Washington. *Geological Society of America Bulletin*, *106*(11), 1413–1429. https://doi.org/10.1130/0016-7606(1994)106%3C1413:PAGOAB%3E2.3.CO;2

Huppert, H., & Woods, A. (2002). The role of volatiles in magma chamber dynamics. *Nature*, *420*(6915), 493–495. https://doi.org/10.1038/nature01211

Ishibashi, H. (2009). Non-Newtonian behaviour of plagioclase-bearing basaltic magma: Subliquidus viscosity measurement of the 1707 basalt of Fuji volcano, Japan. *Journal of Volcanology and Geothermal Research*, *181*(1-2), 78–88. https://doi.org/10.1016/j.jvolgeores.2009.01.004

Jellinek, M. (2014). Volcanic bipolar disorder explained. *Nature Geoscience*, *7*(2), 84–85. https://doi.org/10.1038/ngeo2067

Jentzsch, G., Punongbayan, R., Schreiber, U., Seeber, G., Volksen, C., & Weise, A. (2001). Mayon volcano, Philippines: Changes of monitoring strategy after microgravity and GPS measurements from 1992 to 1996. *Journal of Volcanology and Geothermal Research*, *109*(1-3), 219–234. https://doi.org/10.1016/S0377-0273(00)00313-9

Kaminuma, K. (1966). The crust and upper mantle structure in Japan. Part 2. Crustal structure in Japan from the phase velocity of Rayleigh waves. *Bulletin of the Earthquake Research Institute*, *44*, 495–510.

Kaneko, T., Yasuda, A., Fujii, T., & Yoshimoto, M. (2010). Crypto-magma chambers beneath Mt. Fuji. *Journal of Volcanology and Geothermal Research*, *193*(3-4), 161–170. https://doi.org/10.1016/j.jvolgeores.2010.04.002

Karatson, D., Favalli, M., Tarquini, S., Fornaciai, A., & Worner, G. (2010). The regular shape of stratovolcanoes: A DEM-based morphometrical approach. *Journal of Volcanology and Geothermal Research*, *193*(3-4), 171–181. https://doi.org/10.1016/j.jvolgeores.2010.03.012

Kavanagh, J., & Sparks, R. S. J. (2011). Insights of dyke emplacement mechanics from detailed 3D dyke thickness datasets. *Journal of the Geological Society*, *168*(4), 965–978. https://doi.org/10.1144/0016-76492010-137

Kilburn, C. R. J., & Lopes, R. M. C. (1991). General patterns of flow field growth: Aa and blocky lavas. *Journal of Geophysical Research*, *96*(B12), 19,721–19,732. https://doi.org/10.1029/91JB01924

Koulakov, I., Gordeev, E., Dobretsov, N., Vernikovsky, V., Senyukov, S., Jakovlev, A., & Jakybulatov, K. (2013). Rapid changes in magma storage beneath the Klyuchevskoy group of volcanoes inferred from time-dependent seismic tomography. *Journal of Volcanology and Geothermal Research*, *263*, 75–91. https://doi.org/10.1016/j.jvolgeores.2012.10.014

Lacey, A., Ockendon, J., & Turcotte, D. (1981). On the geometrical form of volcanoes. *Earth and Planetary Science Letters*, *54*(1), 139–143. https://doi.org/10.1016/0012-821X(81)90074-1

Lange, R., Frey, H. M., & Hector, J. (2009). A thermodynamic model for the plagioclase-liquid hygrometer/thermometer. *American Mineralogist*, *94*(4), 494–506. https://doi.org/10.2138/am.2009.3011

Lees, J. (2007). Seismic tomography of magmatic systems. *Journal of Volcanology and Geothermal Research*, *167*, 37–56.

Lister, J., & Kerr, R. (1991). Fluid-mechanical models of crack propagation and their application to magma transport in dykes. *Journal of Geophysical Research*, *96*(B6), 10,049–10,077. https://doi.org/10.1029/91JB00600

Loucks, R. R. (1996). A precise olivine-augite Mg-Fe-exchange geothermometer. *Contributions to Mineralogy and Petrology*, *125*(2-3), 140–150. https://doi.org/10.1007/s004100050211

Lucassen, F., Becchio, R., Harmon, R., Kasemann, S., Franz, G., Trumbull, R., … Dulski, P. (2001). Composition and density model of the continental crust at an active continental margin—The Central Andes between 21° and 27°S. *Tectonophysics*, *341*(1-4), 195–223. https://doi.org/10.1016/S0040-1951(01)00188-3

Mastin, L., Roeloffs, E., Beeler, N., & Quick, J. (2008). Constraints on the size, overpressure, and volatile content of the Mount St. Helens magma system from geodetic and dome-growth measurements during the 2004–2006+ eruption. *United States Geological Survey. Professional Paper*, *1750*, 461–492.

Matthews, S., Sparks, R. S. J., & Gardeweg, M. (1999). The Piedras Grandes–Soncor eruptions, Lascar Volcano, Chile: Evolution of a zoned magma chamber in the Central Andean upper crust. *Journal of Petrology*, *40*(12), 1891–1919. https://doi.org/10.1093/petroj/40.12.1891

Moran, S., Kwoun, O., Masterlark, T., & Lu, Z. (2006). On the absence of InSAR-detected volcano deformation spanning the 1995–1996 and 1999 eruptions of Shishaldin Volcano, Alaska. *Journal of Volcanology and Geothermal Research*, *150*(1-3), 119–131. https://doi.org/10.1016/j.jvolgeores.2005.07.013

Moreno, H., & Gardeweg, M. (1989). La erupción reciente en el complejo volcánico Lonquimay (Diciembre 1988-) Andes del Sur. *Revista Geologica de Chile*, *16*, 93–117.
Morgado, E., Parada, M. A., Contreras, C., Castruccio, A., Gutiérrez, F., & McGee, L. E. (2015). Contrasting records from mantle to surface of Holocene lavas of two nearby arc volcanic complexes: Caburgua-Huelemolle Small Eruptive Centers and Villarrica Volcano, Southern Chile. *Journal of Volcanology and Geothermal Research*, *306*, 1–16. https://doi.org/10.1016/j.jvolgeores.2015.09.023
Munson, B., Young, D. F., & Okiishi, T. H. (1990). *Fundamentals of fluid mechanics*, (3rd ed.), (p. 877). New York: John Wiley.
Murphy, M. D., Sparks, R. S. J., Barclay, J., Carroll, M. R., Lejeune, A. M., Brewer, T. S., … Young, S. (1998). The role of magma mixing in triggering the current eruption at the Soufriere Hills volcano, Monserrat, West Indies. *Geophysical Research Letters*, *25*(18), 3433–3436. https://doi.org/10.1029/98GL00713
Nakamura, M. (1995). Continuous mixing of crystal mush and replenished magma in the ongoing Unzen eruption. *Geology*, *23*(9), 807–810. https://doi.org/10.1130/0091-7613(1995)023%3C0807:CMOCMA%3E2.3.CO;2
Naranjo, J. A., Sparks, R. S. J., Stasiuk, M., Moreno, H., & Ablay, G. (1992). Morphological, structural and textural variations in the 1988–1990 andesite lava of Lonquimay Volcano. Chile. *Geological Magazine*, *129*(06), 657–678. https://doi.org/10.1017/S0016756800008426
Ohmi, S., & Lees, J. (1995). Three-dimensional P- and S-wave velocity structure below Unzen volcano. *Journal of Volcanology and Geothermal Research*, *65*(1-2), 1–26. https://doi.org/10.1016/0377-0273(94)00091-T
Ozerov, A. (2000). The evolution of high-alumina basalts of the Klyuchevskoy volcano, Kamchatka, russia, based on microprobe analyses of mineral inclusions. *Journal of Volcanology and Geothermal Research*, *95*(1-4), 65–79. https://doi.org/10.1016/S0377-0273(99)00118-3
Pinel, V., & Jaupart, C. (2000). The effect of edifice load on magma ascent beneath a volcano. *Philosophical Transactions. Royal Society of London*, *358*(1770), 1515–1532. https://doi.org/10.1098/rsta.2000.0601
Pinel, V., & Jaupart, C. (2004). Magma storage and horizontal dyke injection beneath a volcanic edifice. *Earth and Planetary Science Letters*, *221*(1-4), 245–262. https://doi.org/10.1016/S0012-821X(04)00076-7
Pinel, V., Jaupart, C., & Albino, F. (2010). On the relationship between cycles of eruptive activity and growth of a volcanic edifice. *Journal of Volcanology and Geothermal Research*, *194*(4), 150–164. https://doi.org/10.1016/j.jvolgeores.2010.05.006
Pinkerton, H., & Wilson, L. (1994). Factors controlling the lengths of channel-fed lava flows. *Bulletin of Volcanology*, *56*(2), 108–120. https://doi.org/10.1007/BF00304106
Polanco, E. (2010). Volcanoestratigrafía, geoquímica y peligro volcánico del volcán Lonquimay (38°30′S), Andes del Sur (Chile). PhD Thesis. Universidad de Barcelona, Barcelona, Spain.
Putirka, K. (2008). Thermometers and barometers for volcanic systems. *Reviews in Mineralogy and Geochemistry*, *69*(1), 61–120. https://doi.org/10.2138/rmg.2008.69.3
Rubin, A. (1993). Tensile fracture of rock at high confining pressure: Implications for dyke propagation. *Journal of Geophysical Research*, *98*(B9), 15919–15,935. https://doi.org/10.1029/93JB01391
Shapiro, N. M., Droznin, D. V., Ya, S., Droznina, S. L. S., Gusev, A. A., & Gordeev, E. I. (2017). Deep and shallow long-period volcanic seismicity linked by fluid-pressure transfer. *Nature Geoscience*, *10*(6), 442–445. https://doi.org/10.1038/NGEO2952
Slezin, Y. B. (2003). The mechanism of volcanic eruptions (a steady state approach). *Journal of Volcanology and Geothermal Research*, *122*(1-2), 7–50. https://doi.org/10.1016/S0377-0273(02)00464-X
Sparks, R. S. J. (1993). Genesis y evolucion de magmas. In J. Marti & V. Araña (Eds.) *La volcanologia actual* (in spanish). (p. 578) (pp. 1–44). Madrid: Consejo superior de Investigaciones cientificas.
Sparks, R. S. J., & Cashman, K. V. (2017). Dynamic magma systems: Implications for forecasting volcanic activity. *Elements*, *13*(1), 35–40. https://doi.org/10.2113/gselements.13.1.35
Sparks, R. S. J., Folkes, C., Humphreys, M., Barfod, D., Clavero, J., Sunagua, M., … Pritchard, M. (2008). Uturuncu volcano, Bolivia: Volcanic unrest due to mid-crustal magma intrusion. *American Journal of Science*, *308*(6), 727–769. https://doi.org/10.2475/06.2008.01
Stasiuk, M., & Jaupart, C. (1997). Lava flow shapes and dimensions as reflections of magma system conditions. *Journal of Volcanology and Geothermal Research*, *78*(1-2), 31–50. https://doi.org/10.1016/S0377-0273(97)00002-4
Stasiuk, M., Jaupart, C., & Sparks, R. S. J. (1993). On the variations of flow rate in non-explosive lava eruptions. *Earth and Planetary Science Letters*, *114*(4), 505–516. https://doi.org/10.1016/0012-821X(93)90079-O
Stelling, P., Beget, J., Nye, C., Gardner, J., Devine, J. D., & George, R. M. M. (2002). Geology and petrology of the ejecta from the 1999 eruption of Shishaldin volcano, Alaska. *Bulletin of Volcanology*, *64*, 548–561.
Wadge, G. (1981). The variation of magma discharge during basaltic eruptions. *Journal of Volcanology and Geothermal Research*, *11*(2-4), 139–168. https://doi.org/10.1016/0377-0273(81)90020-2
Walker, G. P. L. (1973). Lengths of lava flows. *Philosophical Transactions. Royal Society of London*, *274*(1238), 107–118. https://doi.org/10.1098/rsta.1973.0030
Walker, G. P. L. (2000). Basaltic volcanoes and volcanic systems. In H. Sigurdsson (Ed.), *Encyclopedia of Volcanoes* (pp. 283–289). San Diego, CA: Academic Press.
White, R., & McCausland, W. (2016). Volcano-tectonic earthquakes: A new tool for estimating intrusive volumes and forecasting eruptions. *Journal of Volcanology and Geothermal Research*, *309*, 139–155. https://doi.org/10.1016/j.jvolgeores.2015.10.020
Wilson, L., Head, J. W., & Parfitt, E. A. (1992). The relationship between the height of a volcano and the depth to its magma source zone: A critical reexamination. *Geophysical Research Letters*, *19*(13), 1395–1398. https://doi.org/10.1029/92GL01073
Wood, C. (1978). Morphometric evolution of composite volcanoes. *Geophysical Research Letters*, *5-6*, 437–439.
Woods, A. (1995). The dynamics of explosive volcanic eruptions. *Reviews of Geophysics*, *33*(4), 495–530. https://doi.org/10.1029/95RG02096
Woods, A. W., & Huppert, H. E. (2003). On magma chamber evolution during slow effusive eruptions. *Journal of Geophysical Research*, *108*(B8). 2403. https://doi.org/10.1029/2002JB002019
Wright, R., Garbeil, H., Baloga, S. M., & Mouginis-Mark, P. J. (2006). An assessment of shuttle radar topography mission digital elevation data for studies of volcano morphology. *Remote Sensing of Environment*, *105*, 41–53.